Journal of Power Sources 196 (2011) 349–354

Contents lists available at ScienceDirect

Journal of Power Sources

journal homepage: www.elsevier.com/locate/jpowsour

Electrochemical behaviour of Sn and Sn–C composite electrodes in LiBOB containing electrolytes

Jusef Hassoun [a,*], Mario Wachtler [b], Margret Wohlfahrt-Mehrens [b], Bruno Scrosati [a]

[a] Department of Chemistry, University of Rome "La Sapienza", Piazzale Aldo Moro, 5, 00185 Rome, Lazio, Italy
[b] Zentrum für Sonnenenergie- und Wasserstoff-Forschung Baden-Württemberg (ZSW), Helmholtzstr. 8, 89081 Ulm, Germany

ARTICLE INFO

Article history:
Received 3 May 2010
Received in revised form 22 June 2010
Accepted 23 June 2010
Available online 1 July 2010

Keywords:
LiBOB
Electrolyte
Sn electrodes
Impedance spectroscopy
Li-ion battery

ABSTRACT

The electrochemical behaviour of Sn electrodes in lithium bis(oxalate)borate (LiBOB)-based electrolyte Li-ion cells is studied by using a carbon-free electrodeposited Sn electrode and a nano-structured Sn–C composite electrode. Cyclic voltammetry, galvanostatic cycling tests, and potentiostatic impedance spectroscopy demonstrate that the presence of carbon promotes the decomposition of the LiBOB-based electrolyte starting at a voltage value of around 1.75 V vs. Li/Li^+. The LiBOB electrolyte decomposition is probably associated with the formation of a high electrode–electrolyte interphase impedance which limits the rate capability. A reduction of the overall impedance and an increase of the electrode rate capability can be achieved by using a pre-treated (pre-lithiated) Sn–C electrode. It is shown that the pre-treatment also reduces the irreversible capacity of the Sn–C electrode and allows to successfully assemble full Li-ion cells.

1. Introduction

The state of art Li-ion batteries commonly involves a graphite anode, a lithium transition metal oxide cathode, and a liquid organic solution electrolyte. Improvements in energy density performance can be obtained by replacing the conventional battery components with others having higher specific capacities. At the anode side very appealing candidates are lithium metal alloys, e.g. Li–Si or Li–Sn alloys, which have theoretical capacities largely exceeding that of graphite, i.e. ca. 4200 mAh g^{-1} and 994 mAh g^{-1}, respectively, vs. 372 mAh g^{-1}, combined with low raw material cost (Si and Sn are abundant resources) and increased safety (the alloys are more stable than graphite in the battery electrolyte medium) [1–3].

We have shown in previous work that a valid approach to make lithium metal alloys successful electrodes in a lithium cell is that of preparing them in form of nanoparticles finely dispersed in a supporting carbon matrix. This gives rise to an apparent micrometer-scale configuration which prevents particle aggregation and avoids safety hazard, while still maintaining the benefit of nano-dimensions in controlling the mechanical strains that typically accompany the charge–discharge process [4,5].

Among new electrolyte salts, a very promising candidate is lithium bis(oxalato)borate (LiBOB). This material has been proposed both as sole electrolyte salt and as electrolyte additive and its compatibility with a large number of different electrode materials has widely been studied (e.g. [6]). It has been shown that LiBOB-based electrolytes have higher stability and higher safety with most electrode materials (except for Co-rich cathodes) but also slightly lower rate capability and lower temperature performance than $LiPF_6$-based electrolytes [7,8]. One important difference to $LiPF_6$ is that LiBOB takes part in the formation of the solid electrolyte interphase (SEI) on the anode [9]. The electrode filming and SEI formation occur in several stages. Most striking is a process occurring at 1.75 V vs. Li/Li^+ which gives rise to additional irreversible capacity. There have been discussions whether this process is related with LiBOB itself or with an intrinsic impurity present in LiBOB electrolytes [7,10]. What is clear is that the irreversible capacity associated with the formation of the SEI, especially with the reduction process occurring at around 1.75 V vs. Li/Li^+, is strongly dependent on the surface area and on the type of the carbon material involved in the electrode mass [7,11] and also on the nature of the electrolyte solvents [12].

To shed further light on the role of the carbon in these interfacial processes the behaviour of LiBOB-based electrolytes has been compared with that of common $LiPF_6$-based electrolyte in Li cells by using carbon-free and carbon-containing electrodes, i.e. electrodeposited Sn [13] and nano-structured Sn–C [4,5] respectively. The results of this study are reported in this work.

2. Experimental

Electrodeposited Sn samples were obtained by electroplating onto a Cu foil in a two-electrode glass cell. An aqueous solution, formed by KCl 0.15 M, $SnCl_2$ 0.175 M, $K_4P_2O_7$ 0.5 M, glycine

* Corresponding author. Tel.: +39 06 49913530; fax: +39 06 491769.
E-mail address: jusef.hassoun@uniroma1.it (J. Hassoun).

0378-7753/$ – see front matter © 2010 Elsevier B.V. All rights reserved.
doi:10.1016/j.jpowsour.2010.06.090

0.125 M and NH_4OH 5 mL L^{-1}, was used as the electrolyte and a Pt foil as the counter electrode. The electroplating current and time conditions were monitored using a Maccor Series 4000 Battery Test System [13]. The Sn–C nano-structured composite anode was prepared according to a procedure already described in one of our laboratories [4,5], that basically involves the infiltration of an organometallic Sn precursor in an organic resorcinol (benzene-1,3-diol)-formaldehyde (methanal) gel, followed by annealing under Ar. Carbon-coated $LiFePO_4$ has been synthesized by combining wet-chemistry and calcination processes as described in a previous work [14].

The Sn–C anode and the $LiFePO_4$ cathode were prepared as thin film electrodes by doctor-blade coating onto a Cu or Al substrate, respectively, of a slurry composed of 80 wt.% active material, 10% PVdF (Solef P6020, Solvay) as binder and 10% carbon black (Super P, MMM Belgium) as electron conductor additive. Sn–C and $LiFePO_4$ films were cut as electrodes of 12 mm diameter with 1.5–2 mg of active material mass and dried under vacuum at 110 °C for 3 h. To compensate for the irreversible capacity of the Sn–C electrode a pre-treatment (partial pre-lithiation) has been carried out by placing the electrode in direct contact with a Li foil wet by standard $LiPF_6$, EC:DMC (1:1) electrolyte for 180 min, as reported previously in one of our laboratories [15].

The $LiPF_6$-based electrolyte of this study was purchased from UBE Industries and used as received. The LiBOB-based electrolyte was prepared from LiBOB salt received from Chemetall GmbH and from battery-grade solvents from UBE Industries.

The cyclic voltammetry and the impedance spectroscopy responses of the Sn-based electrodes were studied using a Biologic VMP3 system as the controlling instrument in a 3 electrode T-cell based on the following configuration: (i) a Sn-based working electrode with a diameter of 1.2 cm, (ii) 1 M $LiPF_6$, EC:PC:DMC (1:1:3 by wt.) or 0.7 M LiBOB, EC:PC:DMC (1:1:3) electrolyte solution soaked on a Whatman glass fibre separator and (iii) Li metal foil counter and reference electrodes. The galvanostatic tests of the Sn-based electrodes were performed using a VMP3 Biologic System as the controlling instrument in a 2 electrode T-cell having a configuration similar to the previous excluding the Li reference.

The cyclic voltammograms of the half cells using Sn-based electrodes have been carried out by varying the cell potential in the range of 0.01 and 2.5 V vs. Li/Li^+ with a scan rate of 0.5 mV s^{-1}.

The electrodeposited Sn and the Sn–C half cells were galvanostatically cycled at a *C*/2 rate (1*C* corresponds to 990 mA g^{-1} and 440 mA g^{-1}, respectively) within 0.005–2 V vs. Li/Li^+. The $LiFePO_4$ half cell was galvanostatically cycled at *C*/3 rate (1*C* corresponds to 170 mA g^{-1}) within 3–4 V vs. Li/Li^+.

The Sn–C/$LiFePO_4$ Li-ion cell was galvanostatically cycled at a *C*/3 and *C*/5 rate (1*C* corresponds to 170 mA g^{-1}) within 2.2–3.8 V. The cell was cathode limited with a mass ratio of anode to cathode active material of 1:1 and the 1*C* rate was referred to the cathode.

Potentiostatic impedance spectroscopy analyses of the Sn-based electrodes have been carried out by using the three electrodes cell configuration including a lithium foil as the counter and the reference electrode, with an amplitude of 10 mV in a frequency range of 75 kHz–10 mHz using a Biologic VMP3 system.

Scanning electron microscopy (SEM) images have been obtained by using a Leo 1450 VP instrument.

3. Results and discussion

Fig. 1 shows a SEM image of the electrodeposited Sn electrode (A) and a SEM image with transmission electron micrograph inset of the Sn–C nano-structured electrode (B).

The electrodeposited Sn exhibits a cauliflower-like morphology [13] with a surface area evaluated to be 5 times larger than the area

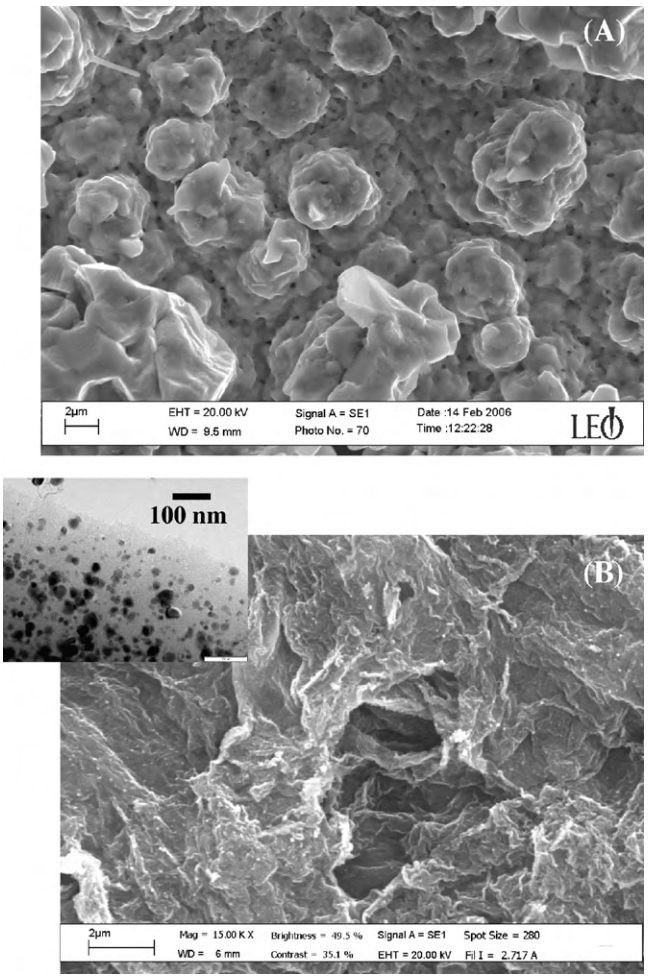

Fig. 1. SEM image of the electrodeposited Sn electrode (A) and SEM image with TEM inset of the Sn–C nano-structured electrode (B) studied in this work.

of the Sn–C electrode. However, as shown by the inset in Fig. 1B, the Sn–C electrode bulk contains nanoparticles of Sn metal dispersed in the carbon matrix. The nanoparticles of Sn are not in direct contact with the electrolyte when the Sn–C is placed in a Li-ion cell, but they may be only indirectly reached by Li-ions through the carbon matrix [5].

Fig. 2A and B compares the cyclic voltammetry response of an electrodeposited Sn electrode using a $LiPF_6$-based and a LiBOB-based EC:PC:DMC (1:1:3 by wt.) electrolyte, respectively.

The main Sn–Li-alloying process, i.e. $Sn + 4.4Li^+ + 4.4e^- \leftrightarrow Li_{4.4}Li$, takes place in the low potential region (below 700 mV vs. Li/Li^+ in the cathodic scan and below 1 V vs. Li/Li^+ in the anodic scan) [2,13]. The irreversible peak at higher voltage around 1.25 V vs. Li/Li^+ is probably related to the reduction of SnO_x traces, $SnO_x + 2xLi^+ + 2xe^- \rightarrow Sn + xLi_2O$, present in the Sn electrode [16].

No further peaks are observed for both the electrolytes. In particular, a peak at 1.75 V vs. Li/Li^+ which has been reported for carbon-based anode materials in LiBOB-based electrolytes [7,11] is here absent.

Fig. 3 shows the result of galvanostatic tests run at a *C*/2 rate of Li cells using an electrodeposited Sn electrode in the $LiPF_6$ (A) and the LiBOB (B)-based electrolytes. The cell voltage vs. specific capacity profiles reveal only plateaus related to the main electrochemical process involving Li-alloying in Sn with no sign of plateaus associated with electrolyte decomposition.

Quite different is the behaviour of the Sn–C electrode. Fig. 4A and B shows the cyclic voltammograms of a Sn–C anode in a $LiPF_6$-based

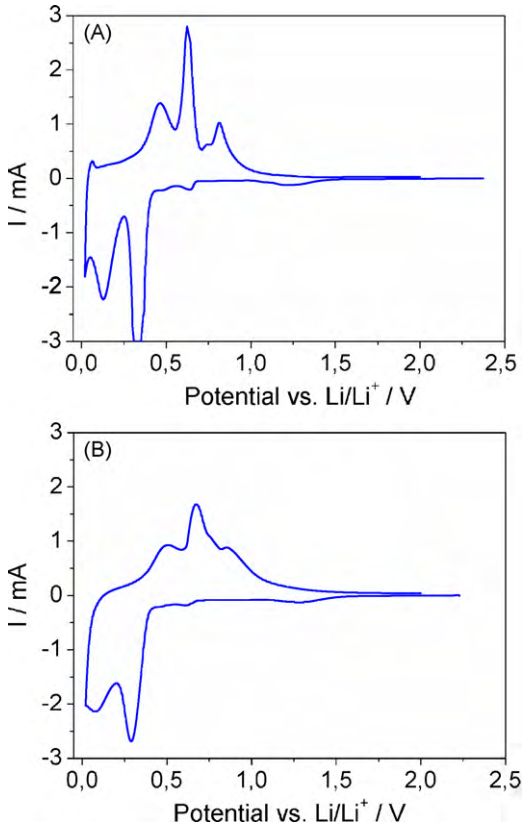

Fig. 2. Cyclic voltammetry profiles of a three electrode cell using electrodeposited Sn as working electrode and Li foil as reference and counter electrodes, where the electrolyte is a $LiPF_6$-based (A) and a LiBOB-based (B) EC:PC:DMC (1:1:3) solution. Scan rate 500 $\mu V\,s^{-1}$.

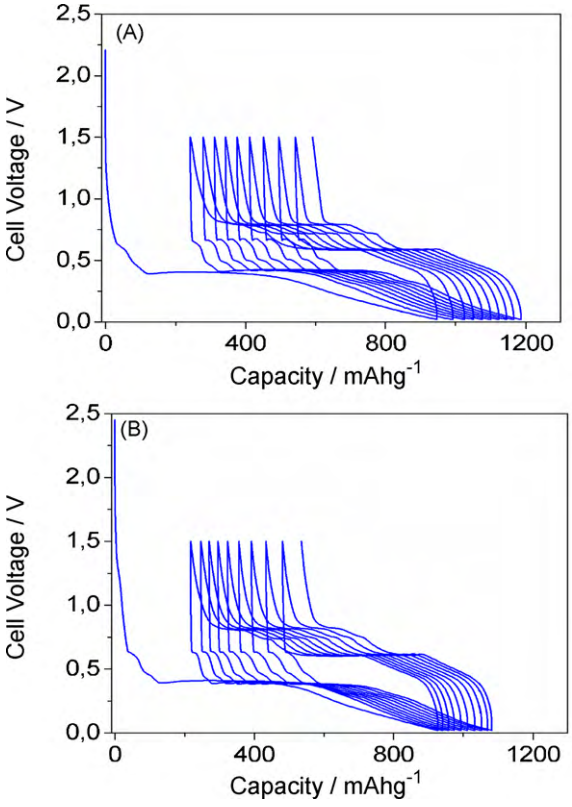

Fig. 3. Voltage vs. specific capacity profiles of a Li cell using electrodeposited Sn, a $LiPF_6$, EC:PC:DMC (1:1:3) electrolyte solution (A) and a LiBOB, EC:PC:DMC (1:1:3) electrolyte solution (B), galvanostatically cycled at $C/2$ rate ($1C = 990\,mA\,g^{-1}$).

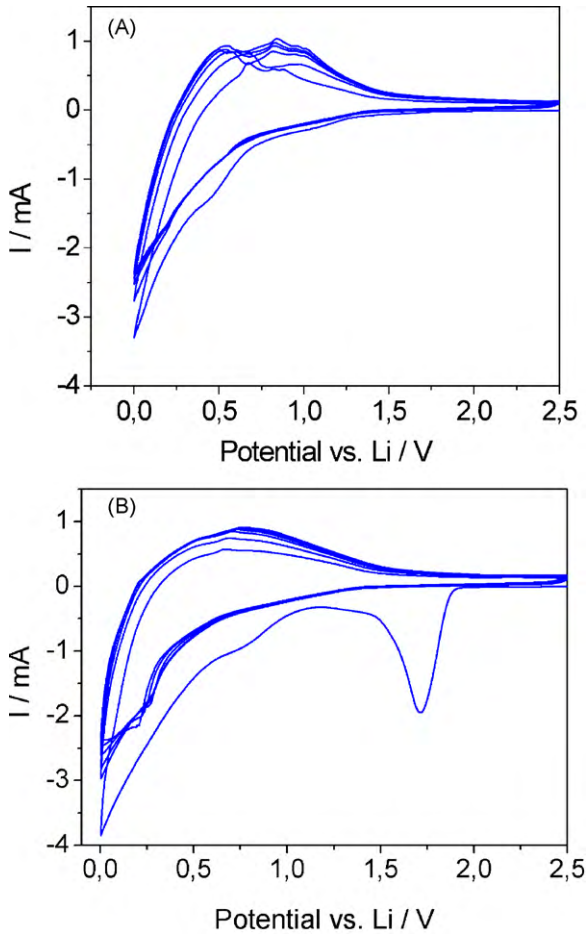

Fig. 4. Cyclic voltammetry profiles of a three electrode cell using nano-structured Sn–C as working electrode and Li foil as reference and counter electrodes, where the electrolyte is a $LiPF_6$-based (A) and a LiBOB-based (B) EC:PC:DMC (1:1:3) solution. Scan rate 500 $\mu V\,s^{-1}$.

and a LiBOB-based EC:PC:DMC (1:1:3 by wt.) electrolyte solution, respectively.

The traces reveal that the alloying process of Li with Sn occurs at low potentials (<700 mV vs. Li/Li^+) with merged profiles due to the nanometric size of Sn [17]. In addition, and at difference from the cell with the $LiPF_6$-based electrolyte, the response in the LiBOB-based electrolyte reveals the appearance of a peak at around 1.75 V vs. Li/Li^+, that may be associated with the decomposition of LiBOB (or of any intrinsic impurity present in the LiBOB-based electrolyte) [7,9–11]. Since this peak is not observed for the carbon-free electrodeposited Sn electrode in LiBOB-based electrolyte (compare Fig. 2B) one can reasonably assume that the process at 1.75 vs. Li/Li^+ is related to the interaction of the LiBOB-based electrolyte with the functional groups present on the surface of carbon. This result is well in line with a previous investigation of $Li_4Ti_5O_{12}$ electrodes in the same type of electrolyte [7]: when the $Li_4Ti_5O_{12}$ electrode was prepared using carbon black as conductive additive a large irreversible capacity associated with the process at 1.75 V vs. Li/Li^+ was observed, which could almost fully be assigned to the carbon black alone. However, when nano-sized Ni powder was used as conductive additive the process at 1.75 V vs. Li/Li^+ was almost fully suppressed [7].

The direct influence of the electrolyte on the performance of the Sn–C electrode is demonstrated in Fig. 5 which reports the voltage vs. specific capacity profiles of Li cells using this electrode in a $LiPF_6$, EC:PC:DMC (A) and a LiBOB, EC:PC:DMC (B) respectively, electrolyte solution.

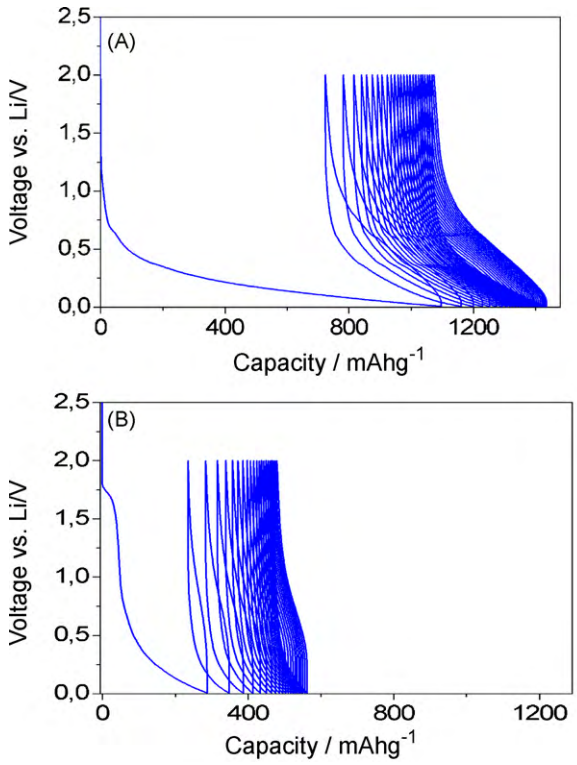

Fig. 5. Voltage vs. specific capacity profiles of a nano-structured Sn–C electrode in a Li cell using a $LiPF_6$, EC:PC:DMC (1:1:3) electrolyte solution (A) and a LiBOB, EC:PC:DMC (1:1:3) electrolyte solution, galvanostatically cycled at a *C*/2 rate ($1C = 440\,mA\,g^{-1}$).

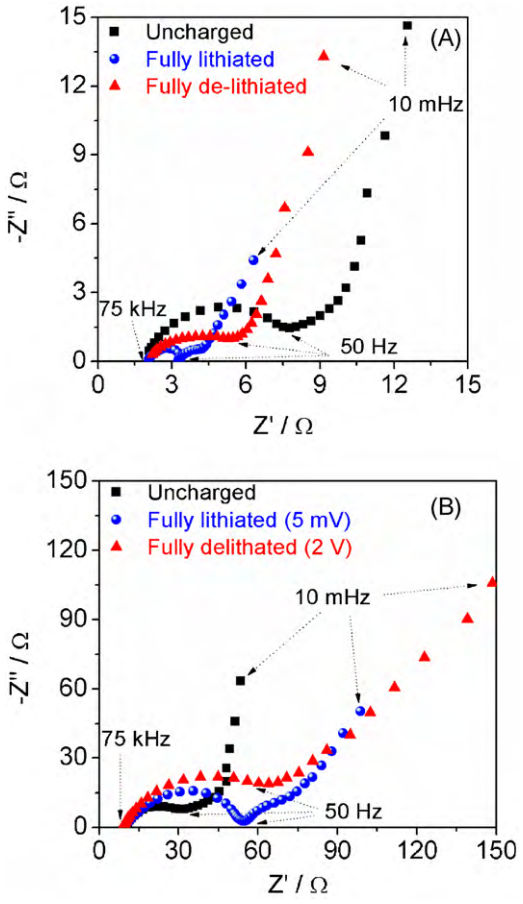

Fig. 6. Nyquist plots of potentiostatic electrochemical impedance spectra (P-EIS) of a three electrode cell using electrodeposited Sn as working electrode, Li foil as reference and counter electrodes, and a $LiPF_6$, EC:PC:DMC (1:1:3) (A) and a LiBOB, EC:PC:DMC (1:1:3) (B) electrolyte solution. Frequency range: 75 kHz–10 mHz. Applied signal: 10 mV. The spectra at the lithiated and unlithiated states have been recorded after galvanostatic charge/discharge at a *C*/2 rate.

While the $LiPF_6$-based half cell shows the classic response of the Sn–C electrode, with an associated specific capacity of the order of 400 mAh g^{-1} (Fig. 5A), that using the LiBOB-based electrolyte reveals the above discussed plateau at about 1.75 V vs. Li/Li^+ and the reversible specific capacity is depressed to about 100 mAh g^{-1} (Fig. 5B). This difference in behaviour is ascribed to differences in the electrode–electrolyte interphase in the two media as confirmed by potentiostatic electrochemical impedance spectroscopy (P-EIS) carried out on cells at different charge–discharge states.

Fig. 6 shows the Nyquist plots of a cell using the Sn–C electrode as the working electrode in a $LiPF_6$, EC:PC:DMC (A) and in a LiBOB, EC:PC:DMC (B) electrolyte solution.

The general response is qualitatively described in terms of medium to high frequency semicircles associated with SEI film and charge transfer, followed by a low frequency tilted line likely corresponding to cell capacitance [18,19]. To properly interpret the responses, the data were analyzed by a Non-Linear Least-Square (NLLSQ) fit software developed by Boukamp [20,21]. The used equivalent circuits, in Boukamp notation, were of the type $R(RQ)Q$ in the case where only one semicircle was observed in the impedance Nyquist plots, and $R(RQ)(RQ)Q$ in the case where two semicircles were observed, with R denoting a resistance and Q a capacitance. The quality of the fit was confirmed by a chi-square (χ^2) factor of the order of 10^{-4}, which is considered acceptable for the validity of the proposed circuitry model. The results of this analysis are summarized in Table 1.

At the high frequency region (50 Hz–75 kHz) the semicircle associated with a native film present at the electrode is observed for the uncharged (pristine) state. The formation of such a native film upon first contact of the electrodes with the electrolyte has been previously reported [22]. The associated film resistance R_f is of the order of 8 Ω for the Sn–C electrode in $LiPF_6$ electrolyte, that increases to 36 Ω in the case of LiBOB electrolyte. This difference is associated with the formation of different film layers depending on the electrolyte, in particular on the different salts, in contact with the Sn–C electrode. It has been demonstrated in several papers that the nature of the formed film strongly depends not only on the electrolyte solvent but also on the dissolved lithium salt [23] and it is known that LiBOB takes actively part in the filming process [9].

In the fully lithiated state the SEI resistance decreases to a value of 1 Ω for the Sn–C electrode in the $LiPF_6$-based electrolyte. This

Table 1
SEI film resistance (R_f) and charge transfer resistance (R_{ct}) for the Sn–C and the pre-treated Sn–C electrodes at various states of charge. The cells were galvanostatically cycled at a *C*/2 rate ($1C = 0.44\,A\,cm^{-2}$) using $LiPF_6$, EC:PC:DMC (1:1:3) or LiBOB, EC:PC:DMC (1:1:3) electrolyte solutions.

	R_f/Ω	R_{ct}/Ω
Sn–C/$LiPF_6$		
Uncharged	8	–
Lithiated	1	1
Delithiated	5	–
Sn–C/LiBOB		
Uncharged	36	–
Lithiated	45	20
Delithiated	52	–
Li–SnC/LiBOB		
Uncharged	40	22
Lithiated	35	8
Delithiated	40	–

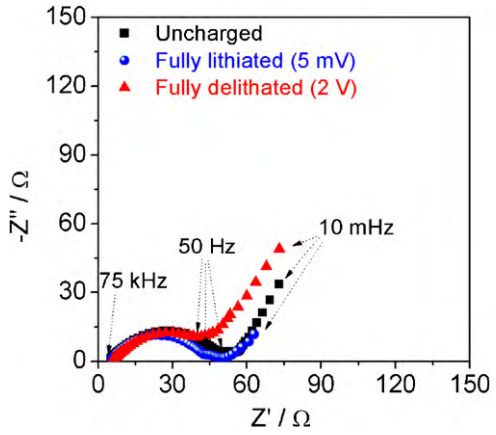

Fig. 7. Nyquist plots of potentiostatic electrochemical impedance spectra (P-EIS) of a three electrode cell using a pre-treated nano-structured Sn–C as working electrode, Li foil as reference and counter electrodes, and a LiBOB, EC:PC:DMC (1:1:3) electrolyte solution. Frequency range: 75 kHz–10 mHz. Applied signal: 10 mV. The spectra at the lithiated and unlithiated states have been recorded after galvanostatic charge/discharge at a *C*/2 rate.

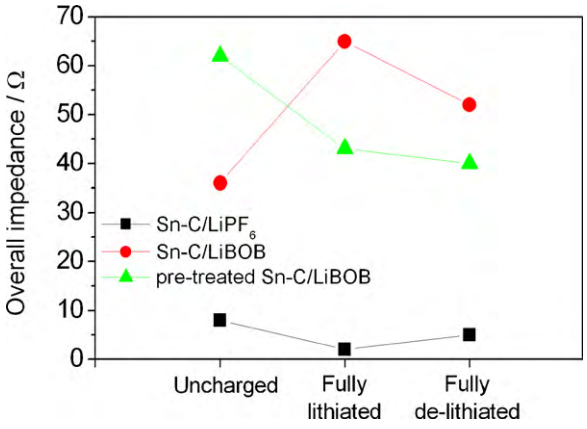

Fig. 8. Overall electrode–electrolyte impedance values of the pristine Sn–C and of the pre-treated Sn–C electrodes in the LiBOB-based electrolyte at the various states of charge in comparison with the impedances of the pristine Sn–C electrode in the $LiPF_6$-based electrolyte at the same states of charge. For further details see Table 1.

could be due to the alloying between Li and Sn, involving a surface area increase which is in inverse proportion to the impedance [24]. In addition, it has been observed for graphite electrodes that a relatively resistive preliminary film, present at the beginning of the first charge is transformed into a highly conductive SEI at low potentials (vs. Li/Li^+) [25]. At the contrary, the SEI resistance increases to a value of the order of 45 Ω in the LiBOB-based electrolyte. This resistance increase has been associated with the LiBOB decomposition at 1.75 V vs. Li/Li^+ [25,26]. In the fully lithiated state an additional semicircle associated with the charge transfer is observed at the medium frequency range (0.1 Hz–50 Hz). As expected from the difference in SEI, a smaller charge transfer resistance R_{ct} is observed for the $LiPF_6$-based electrolyte than for the LiBOB-based electrolyte, i.e. 1 Ω and 20 Ω. For the 2 V fully delithiated electrodes only one semicircle, probably associated with the SEI is observed. In agreement with results from other authors [27] a small increase of the resistance to a value of 5 Ω is observed for the electrode in the $LiPF_6$-based electrolyte. Different is the behaviour of the SEI for the electrode in LiBOB-based electrolyte, with a resistance value increasing to 52 Ω, a value higher than that observed in the uncharged state. The high SEI resistance of the Sn–C electrode in LiBOB electrolyte causes a reduction of the reversible capacity achieved at the actual *C*-rate (cf. above).

Important information is provided by the impedance study performed on a Li half cell cycled galvanostatically at *C*/2 rate using a pre-treated SnC electrode (see experimental section) [15] in combination with the LiBOB-based electrolyte, see Fig. 7. Also these impedance data have been analyzed by the NLLSQ fit software using equivalent circuits of the types $R(RQ)Q$ and $R(RQ)(RQ)Q$ with a chi-square (χ^2) of 10^{-4} as quality control. The results are summarized in Table 1.

Since even in the uncharged state the Sn–C electrode is partially lithiated, both the SEI and the charge transfer semicircles are observed as for the fully lithiated state, while in the fully delithiated state only the SEI semicircle is observed. The SEI impedance value for the uncharged state is 40 Ω which is slightly higher than the one observed for the uncharged pristine Sn–C electrode in LiBOB electrolyte. The SEI impedance value of the pre-treated Sn–C decreases to 35 Ω in the fully lithiated state and then returns to 40 Ω in the fully delithiated state.

The overall electrode impedance trends discussed above are compared in Fig. 8. The Sn–C electrode shows smaller impedance values with the $LiPF_6$-based electrolyte compared to the LiBOB-based one, due to the different nature of the formed SEI [9]. Furthermore, the pre-treated Sn–C electrode shows a smaller impedance value at the fully lithiated state than the pristine Sn–C electrode, i.e. 43 Ω vs. 65 Ω, respectively, see Table 1 and Fig. 8. Due to the pre-lithiation of the Sn–C, the cell exhibits an open circuit potential of approximately 450 mV vs. Li/Li^+. Since this potential level is lower than that of the major part of the electrolyte decomposition and of SEI filming, these processes occur spontaneously (chemical reaction) as soon as the electrode gets into contact with the electrolyte during cell assembly.

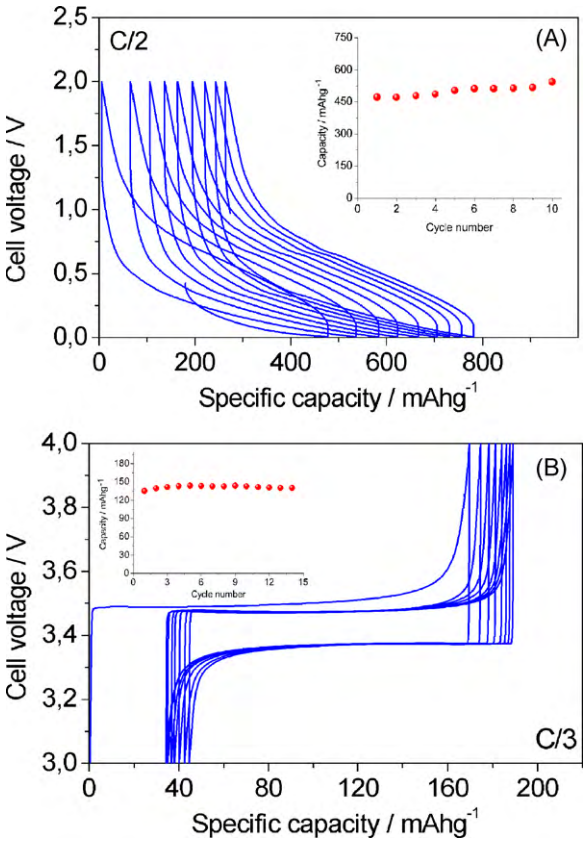

Fig. 9. Voltage vs. specific capacity profiles and reversible capacity vs. cycle number plots (in inset) of galvanostatic tests performed on Li cells using a pre-treated nano-structured Sn–C electrode (A) or a $LiFePO_4$ electrode (B), and a LiBOB, EC:PC:DMC (1:1:3) electrolyte solution. A *C*/2 rate has been used for Sn–C ($1C = 440\ mA\ g^{-1}$) and a *C*/3 rate for $LiFePO_4$ ($1C = 170\ mA\ g^{-1}$).

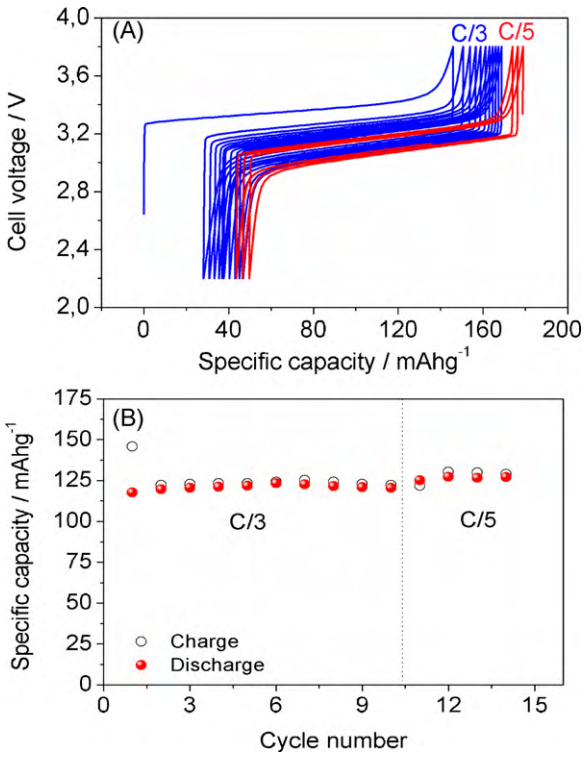

Fig. 10. Voltage vs. specific capacity profile (A) and specific capacity vs. cycle number plot (B) of a Li-ion battery using a pre-treated Sn–C anode, a $LiFePO_4$ cathode, and a LiBOB, EC:PC:DMC (1:1:3) electrolyte solution, galvanostatically cycled at a *C*/3 rate ($1C = 170\,mA\,g^{-1}$).

The low values of SEI and charge transfer resistances have a direct effect on the electrochemical behaviour of the electrode. This is demonstrated in Fig. 9A, that reports the cell voltage vs. specific capacity profile of the half cell using the pre-treated Sn–C electrode in the LiBOB-based electrolyte. Due to the lower electrode impedance (see Fig. 7 and Table 1) the observed reversible capacities of the pre-treated Sn–C are higher than those of the pristine Sn–C, i.e. about $470\,mAh\,g^{-1}$ vs. $100\,mAh\,g^{-1}$, at the same *C*-rate, compare Figs. 5B and 9A. In addition, a small increase of the reversible capacity is observed during the first cycles, as reported in the inset of Fig. 9A. This may be attributed to some structural reorganisation in the Sn–C electrode and also to a further decrease of the overall impedance value during the cycling test which helps the low voltage alloying processes.

Considering its favourable behaviour, the pre-treated Sn–C electrode was used to assemble a full lithium ion cell using LiBOB-based electrolyte. The cell was completed with a $LiFePO_4$ cathode [14,28]. Before cell assembly the $LiFePO_4$ cathode was separately studied in a Li half cell to test its response in the LiBOB-based electrolyte. Fig. 9B shows the voltage vs. specific capacity of a charge–discharge cycles of this $LiFePO_4$ half cell and, as inset, the cycling behaviour of the reversible capacity. The figure evidences a stable reversible capacity of about $140\,mAh\,g^{-1}$, i.e. 82% of the theoretical value for the $LiFePO_4$ electrode. In addition the voltage develops around the expected 3.5 V value, and the first cycle irreversibility corresponds to approximately 20% of the charge capacity.

Once ascertained its favourable response, the $LiFePO_4$ cathode was coupled with the pre-treated Sn–C anode in the LiBOB-based electrolyte to form a complete lithium ion battery configuration. The cell was galvanostatically cycled at two different *C*-rates, i.e. *C*/3 and *C*/5 ($1C = 170\,mA\,g^{-1}$, referred to the active mass of the cathode). Fig. 10 reports the voltage vs. specific capacity (A) and the specific capacity vs. cycle number (B) of this Li-ion cell. A stable capacity of around $125\,mAh\,g^{-1}$ was observed at both current rates. It is slightly smaller than the capacity of the $LiFePO_4$ half cell (Fig. 9B) which may be related with differences in the overall impedances between full cell and half cell. The initial irreversible capacity (of the full cell) of $28\,mAh\,g^{-1}$ (approximately 20% of the charge capacity) reflects the value associated with the $LiFePO_4$ electrode, see Fig. 9B. The cell voltage of the Li-ion cell here reported, i.e. 3 V, combined with its value of the specific capacity, is expected to result in a value of energy density that compares well with those of conventional lithium ion batteries.

4. Conclusions

In this work we demonstrated that the presence of carbon promotes the decomposition of the LiBOB-based electrolyte with the formation of a high impedance electrode–electrolyte interphase that in turn limits the rate capability. It was also shown that a pre-treatment of the Sn–C composite electrode, i.e. a partial pre-lithiation, causes a reduction of the overall impedance, this resulting in an increase of the electrode rate capability. The Sn–C pre-lithiated electrodes can be successfully used as anodes, in combination with $LiFePO_4$ cathode and LiBOB-based electrolyte, to form a complete lithium ion battery. The results reported in this paper demonstrate the promising behaviour of this battery and work is in progress in our laboratories to further optimize its performances to a level eventually suitable for electric vehicles application.

Acknowledgements

This work has been carried out in the framework of the University of Ulm-University of Rome Sapienza Internationalization project. Chemetall GmbH (Germany) is gratefully acknowledged for providing LiBOB salt.

References

[1] J.R. Dahn, R.E. Mar, A. Abouzeid, J. Electrochem. Soc. 153 (2006) A361.
[2] M. Wachtler, M. Winter, J.O. Besenhard, J. Power Sources 105 (2002) 151.
[3] J. Yang, M. Wachtler, M. Winter, J.O. Besenhard, Electrochem. Solid-State Lett. 2 (1999) 161.
[4] G. Derrien, J. Hassoun, S. Panero, B. Scrosati, Adv. Mater. 19 (2007) 2336.
[5] J. Hassoun, G. Derrien, S. Panero, B. Scrosati, Adv. Mater. 20 (2008) 3169.
[6] Z.H. Chen, W.Q. Lu, J. Liu, K. Amine, Electrochim. Acta 51 (2006) 3322.
[7] M. Wachtler, M. Wohlfahrt-Mehrens, S. Ströbele, J.-C. Panitz, U. Wietelmann, J. Appl. Electrochem. 36 (2006) 1199.
[8] K. Xu, B. Deveney, K. Nechev, Y.F. Lam, R.T. Jow, J. Electrochem. Soc. 155 (2008) A959.
[9] K. Xu, S.S. Zhang, T.R. Jow, Electrochem. Solid-State Lett. 6 (2003) A117.
[10] K. Xu, S.S. Zhang, R. Jow, J. Power Sources 143 (2005) 197.
[11] J.-C. Panitz, U. Wietelmann, M. Wachtler, S. Ströbele, M. Wohlfahrt-Mehrens, J. Power Sources 153 (2006) 396.
[12] K. Xu, J. Electrochem. Soc. 155 (2008) A733.
[13] J. Hassoun, S. Panero, P. Reale, B. Scrosati, Int. J. Electrochem. Sci. 1 (2006) 110.
[14] G. Arnold, J. Garche, R. Hemmer, S. Ströbele, C. Vogler, M. Wohlfahrt-Mehrens, J. Power Sources 119–121 (2003) 247.
[15] J. Hassoun, P. Reale, S. Panero, B. Scrosati, Adv. Mater. 21 (2009) 4807.
[16] J. Chouvin, J. Olivier-Fourcade, J.C. Jumas, B. Simon, P. Biensan, F.J. Fernandez Madrigal, J.L. Tirado, C. Perez Vicente, J. Electroanal. Chem. 494 (2000) 136.
[17] L.F. Nazar, G. Goward, F. Leroux, M. Duncan, H. Hung, T. Kerr, J. Gaubicher, Int. J. Inorg. Chem. 3 (2001) 191.
[18] D. Aurbach, B. Markovsky, M.D. Levi, E. Levi, A. Schechter, M. Moshkovich, Y. Cohen, J. Power Sources 81–82 (1999) 95.
[19] J.R. McDonald, Impedance Spectroscopy, Wiley, New York, 1987.
[20] B.A. Boukamp, Solid State Ionics 18 (1986) 136.
[21] B.A. Boukamp, Solid State Ionics 20 (1986) 31.
[22] D. Aaurbach, J. Power Sources 89 (2000) 206.
[23] S. Leroy, H. Martinez, R. Dedryvère, D. Lemordant, D. Gonbeau, Appl. Surf. Sci. 253 (2007) 4895.
[24] J.R. Macdonald, Impedance Spectroscopy, Wiley, 1987.
[25] S.S. Zhang, K. Xu, T.R. Jow, Electrochim. Acta 51 (2006) 1636.
[26] Z. Chen, W.Q. Lu, J. Liu, K. Amine, Electrochim. Acta 51 (2006) 3322.
[27] E. Markevich, E. Pollak, G. Salitra, D. Aurbach, J. Power Sources 174 (2007) 1263.
[28] P. Reale, S. Panero, B. Scrosati, J. Garche, M. Wohlfahrt-Mehrens, M. Wachtler, J. Electrochem. Soc. 151 (2004) A2138.